# Non-Korringa nuclear relaxation in the ferromagnetic phase of the bilayered manganite $La_{1.2}Sr_{1.8}Mn_2O_7$

M. J. R. Hoch,[1] P. L. Kuhns,[1] W. G. Moulton,[1] Jun Lu,[1] A. P. Reyes,[1] and J. F. Mitchell[2]
[1]*National High Magnetic Field Laboratory, Florida State University, 1800 E. Paul Dirac Drive, Tallahssee, Florida 32310, USA*
[2]*Materials Science Division, Argonne National Laboratory, Argonne, Illinois 60439, USA*
(Received 18 December 2008; revised manuscript received 7 May 2009; published 13 July 2009)

In contrast to ferromagnetic (FM) three-dimensional manganites, $^{55}$Mn NMR spectra obtained for the FM phase of the colossal magnetoresistance bilayer manganite $La_{1.2}Sr_{1.8}Mn_2O_7$ show a broad distribution of hyperfine fields at Mn sites. The hyperfine distribution reflects variations in the electronic structure at the local level. $^{55}$Mn spin-lattice relaxation rates have a surprisingly weak dependence both on temperature and on applied magnetic field. Significant departures of the relaxation rate from Korringa temperature dependence below 40 K provide evidence for nonFermi liquid behavior in this quasi-two-dimensional metal. At temperatures approaching $T_C$ from below, in the range where colossal magnetoresistance appears, further anomalous and field-dependent behavior is found in the relaxation rate temperature dependence. The results provide evidence for changes in the electronic structure with temperature in this poorly metallic system. At low temperatures the changes are possibly linked to orbital ordering effects. In addition, statistical fluctuations in dopant concentration may play some role in inducing local variations in the electronic structure. Above 90 K the emergence of polarons is likely to be responsible for the observed decrease in the relaxation rate.

DOI: 10.1103/PhysRevB.80.024413 PACS number(s): 75.30.−m, 75.47.Lx, 76.60.Jx

## I. INTRODUCTION

The bilayered manganites $La_{2-2x}Sr_{1+2x}Mn_2O_7$ exhibit interesting and challenging magnetoelectronic properties, including colossal magnetoresistance (CMR), that involve spin, charge, and orbital ordering.[1–6] The crystal structure consists of perovskite $[(La_{1-x}Sr_x)MnO_3]_2$ bilayers separated by insulating nonmagnetic blocking rocksalt layers of $[(La_{1-x}Sr_x)O]$ in a body-centered tetragonal structure with the layers stacked along the $c$ axis. For $x$ in the intermediate doping regime ($0.32<x<0.40$) the ground state is ferromagnetic (FM) with a Curie temperature $T_C>100$ K, which is dependent on $x$ and to some extent on sample quality. The high-temperature phase is designated as paramagnetic (PM) insulating.[1,7,8] A metal-insulator transition accompanies the magnetic transition at $T_C$. CMR is found for $T$ close to $T_C$ with maximum effect (20 000%) occurring for $x=0.4$.[1] Jahn-Teller (JT) distortions in the PM phase localize carriers producing magnetoelastic polarons that play an important role in determining the high-temperature properties of the material.[9–15] A number of investigations have suggested that JT effects continue to play a role in the FM phase[10,11,15] but x-ray and neutron-scattering results show the disappearance of diffuse scattering disorder below $T_C$, which is interpreted as polaron collapse at the phase transition.[9] It has been argued that polaron ordering in the FM phase can account for the disappearance of diffuse scattering.[15] The presence or absence of polarons in the FM phase is not yet firmly established.

The low-$T$ FM phase has been described as a fully spin-polarized two-dimensional (2D) electron system with $e_g$ electron transfer between Mn ions due to the double-exchange (DE) mechanism.[9,10] The reduced dimensionality enhances spin and charge fluctuations as $T$ is increased. Neutron-scattering experiments on single-crystal samples show that the FM two-layer system is reasonably well described by the Heisenberg model allowing for anisotropic intrabilayer and weak interbilayer exchange interactions.[16–18] In order to account for observed changes in the relative importance of the $d_{x^2-y^2}$ and $d_{3z^2-r^2}$ orbitals with $x$, and taking into account the observed tetragonal symmetry of the lattice, an orbital liquid state has been proposed, which is consistent with strong electron correlation effects in the system.[18]

Information on the 2D character of the Fermi surface has been obtained both from theoretical calculations and, experimentally, using various techniques including magnetic Compton scattering and angle-resolved photoemission spectroscopy (ARPES).[19–22] Some similarities to the Fermi surfaces of high-$T_C$ cuprates have been noted with Fermi arc and pseudogap features.[21,22] The spectral weight at $E_F$ is found to be very small and this is attributed to strong electron-lattice coupling.[22] Weak localization effects have been considered for layered systems such as the cuprates and layered manganites using a quasi-2D model.[23] For $La_{2-2x}Sr_{1+2x}Mn_2O_7$ the magnetoresistance behavior with applied field is found to be consistent with this model in the three-dimensional (3D) anisotropic metal limit at low temperatures.[23]

Muon spin rotation experiments reveal that the correlation time for local-field fluctuations increases as $T_C$ is approached from above and becomes very long and roughly constant below $T_C$.[24] A distribution of spin-lattice relaxation rates is found giving rise to stretched exponential form for the relaxation function that points to an inhomogeneous distribution of correlation times for the polaron dynamics.[24,25] The muon spin rotation results suggest that the polarons are much larger than in 3D manganites. Previous NMR work on this material has focused on spectral lineshapes. Zero field (ZF) and low-field $^{55}$Mn spectra have been obtained at liquid-helium temperatures in both single crystal[26] and polycrystalline[27] samples, while ZF and in-field $^{139}$La spectra measurements have been made on crushed single crystals over a wide range

 

of temperature.[28] The $^{139}$La spectra have been interpreted as providing evidence for field-induced ferromagnetism at temperatures above $T_C$.[28] No previous NMR relaxation rate measurements appear to have been made on this material. The present experiments have used zero-field and low-field $^{55}$Mn ferromagnetic NMR relaxation methods to probe the dynamics of the metallic phase of $La_{1.2}Sr_{1.8}Mn_2O_7$. Open questions for this system include the presence or absence of polarons in the FM phase and the importance of effects such as weak localization and electron-electron interaction at low temperatures.

## II. EXPERIMENTAL DETAILS

The $x=0.4$ single-crystal sample was cut from a larger crystal grown in a floating-zone furnace. NMR spin-echo experiments were carried out in zero field and in fields up to 10 T using a computer-controlled variable frequency spectrometer with auto tuning capability. $^{55}$Mn spectra were obtained by integrating spin echoes as a function of frequency. Relaxation rate measurement procedures are described below. Averaging was used to improve the signal-to-noise ratio particularly at higher temperatures. Because the electrical conductivity is roughly two orders of magnitude lower along the $c$ axis direction than in the $ab$ plane,[1] the rf coil axis was directed parallel to the $ab$ plane to minimize skin depth effects. Estimates of the skin depth $\delta$ give values much less than 100 microns at 4 K increasing to greater than 1 mm at 120 K with a rapid increase with $T$ occurring between 100 and 120 K corresponding to the decrease in electrical conductivity by roughly two orders of magnitude in this temperature range. The sample is roughly half cylindrical in shape with dimensions $3.4\times2.6$ mm in the cleaved basal $ab$ plane and height parallel to $c$ of 1.4 mm. $^{55}$Mn signals could be observed both in ZF and in higher fields at temperatures over the range of 2–200 K in the single-crystal sample. The signals at temperatures above $T_C$ are attributed to small amounts of 3D manganite intergrowth phase,[7,27] with a concentration estimated from magnetization measurements of ~0.2%. This phase could be observed because of the large signal enhancement factor in ferromagnets. It has been suggested that differences in the measured $T_C$ values for different samples may be due to different concentrations of intergrowth.[27] The single-crystal sample used in the present experiments is of high quality with low intergrowth concentration. Magnetization measurements were made as a function of temperature $T$ and applied field $H$ in a Quantum Design vibrating sample magnetometer. Figure 1(a) shows $M$ versus $T$ for $B=\mu_0 H$ fields of 1 and 7 T along the $c$ axis while Fig. 1(b) shows $M$ versus $T$ for the same fields with $H$ in the $ab$ plane. Figure 1(c) shows $M$ versus $H$ at 4.1 K for the two crystal orientations. As can be seen $M$ saturates for $\mu_0 H_{ab}>0.2$ T at 4.1 K and there is some difference in the $M$ dependence on $H$ and $T$ in the two orientations, due to the anisotropy of the system, with preferred ordering of the magnetic moments in the $ab$ plane. Most of the NMR measurements were carried out in applied fields of either 1 or 3 T with additional spectra recorded in the range of 0–6 T.

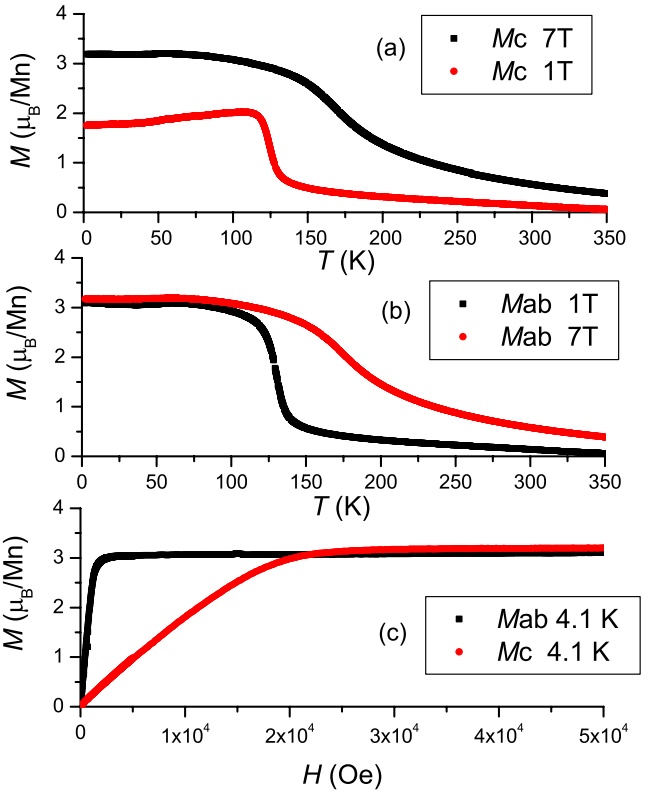


FIG. 1. (Color online) (a) and (b) Magnetization $M$ versus $T$ for single crystal $La_{1.2}Sr_{1.8}Mn_2O_7$ with applied fields $\mu_0 H=1$ and 7 T parallel to the crystal $c$ axis [1(a)] and $\mu_0 H=1$ and 7 T in the $ab$ plane [1(b)]. (c) $M$ versus $H$ for the two applied field orientations at 4.1 K.

## III. RESULTS

### A. NMR spectra

Figure 2 shows the magnetic field dependence of $^{55}$Mn spectra at 4 K with $\mu_0 H$, in the range of 0 to 6 T, applied in the $ab$ plane. The broad spectra show little change in shape or position until the field exceeds 1 T. The spectral amplitudes, which decrease with increasing $H$, have been normalized for clarity. Similar behavior is obtained for $H$ along $c$. In addition to the $^{55}$Mn spectra for the $x=0.4$ bilayer crystal in Fig. 2(a) $^{55}$Mn spectrum obtained in an applied field of 3 T for an $x=0.3$ sample of 3D $La_{1-x}Sr_xMnO_3$ (LSMO) at 10 K (Ref. 32) is shown for comparison.

Figure 3(a) ($H$ along $c$) and Fig. 3(b) ($H$ in $ab$ plane) show representative spectra for the two bilayer crystal orientations as a function of temperature in an applied field of 1 T with the spectral amplitudes normalized. The vertical dashed lines indicate the center frequency, given by the first moment, for each spectrum. The frequency shifts with $T$ are comparatively small consistent with the small changes in the magnetization below 100 K shown in Fig. 1. The spectra are fitted with multiple (three to five) Gaussian components as shown in Fig. 3. As can be seen, two components are generally of dominant importance. No constraints were placed on amplitudes or widths of the Gaussian components in the fitting procedure.

To avoid complications due to the presence in this system of both the intergrowth phase and domain walls,[29–31] both of

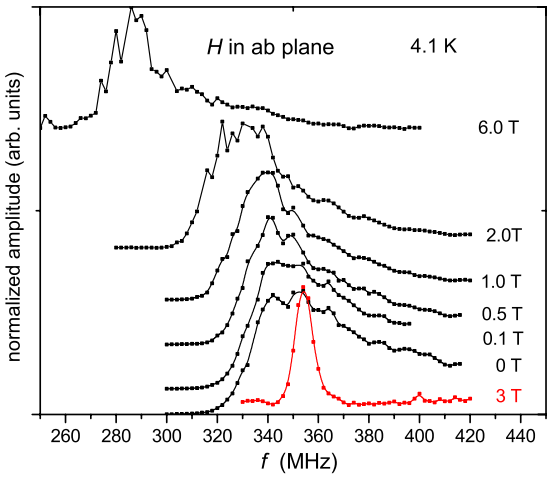


FIG. 2. (Color online) $^{55}$Mn NMR frequency scan spectra for single crystal $La_{1.2}Sr_{1.8}Mn_2O_7$ (plotted points) at $T$=4.1 K in applied fields from 0 to 6 T in the *ab* plane. The spectra shift to lower frequencies as the field increases above 1.0 T consistent with saturation of the magnetization as domain walls are swept out. The hyperfine field at $^{55}$Mn sites is clearly directed antiparallel to the applied field. The much narrower spectrum for the 3D manganite $La_{0.7}Sr_{0.3}MnO_3$ (red curve) obtained at 10 K in a field of 3 T (Ref. 32) is shown for comparison.

which can make a disproportionally large contribution to observed ZF spectra because of large signal enhancement effects, the temperature dependence of spectra was studied in saturating applied fields of 1–3 T. The FM signal enhancement factor within domains, given by $\eta=H_{hf}/(H_{anis}+H)$, where $H_{anis}$ is the anisotropy field and $H$ the applied field, is typically large ($\sim 10^3$). In 3D FM the enhancement factor in domain walls is typically one to two orders of magnitude higher than this. Figure 4 shows the reduced enhancement

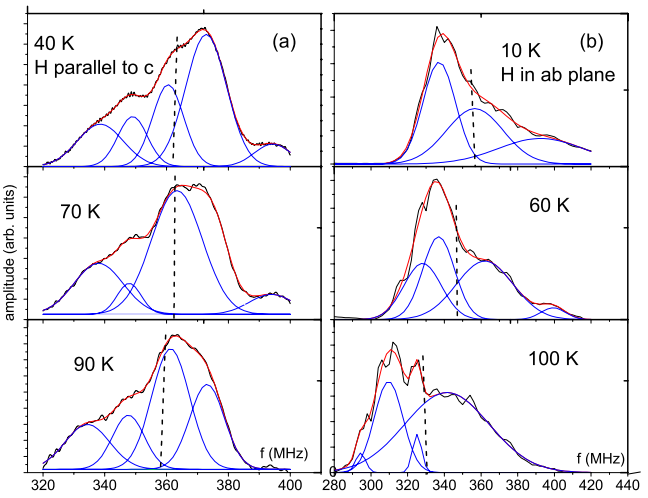


FIG. 3. (Color online) $^{55}$Mn NMR spectra for single crystal $La_{1.2}Sr_{1.8}Mn_2O_7$ (a) at temperatures in the range from 10 to 120 K in an applied field of 1 T in the *ab* plane; (b) at temperatures in the range from 40 to 120 K in a field of 1 T along the *c* axis. The amplitudes of all spectra have been normalized to facilitate the comparison of shapes. The fitted Gaussian curves suggest nonequivalent Mn sites as discussed in the text.

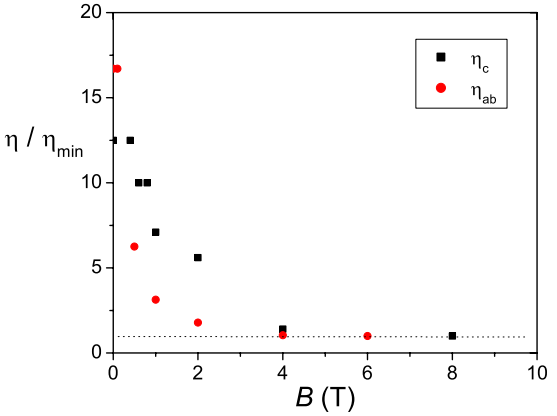


FIG. 4. (Color online) The ratio of $^{55}$Mn enhancement factors $\eta/\eta_{min}$ in $La_{1.2}Sr_{1.8}Mn_2O_7$, with $\eta_{min}$ the enhancement factor measured at 8 T, as a function of applied field directed parallel to *c* (black squares) and in the *ab* plane (red circles). The dashed line at $\eta/\eta_{min}=1$ shows the high-field limit.

factor $\eta/\eta_{min}$ as a function of applied field at 4.1 K, with $\eta_{min}(\sim 3)$ the enhancement observed in high field. The ratio $\eta/\eta_{min}$ is reduced by more than an order of magnitude in fields that sweep out domain walls and saturate $M$. The center frequencies of the spectra are observed to shift to lower values as $H$ is increased, consistent with the hyperfine field being aligned antiparallel to the applied field. Note that, as expected, the shift does not depend linearly on $H$ until $M$ is saturated.

Taking data in fields sufficiently large to produce saturation of the magnetization has the added advantage of reducing the high-frequency magnetic permeability of the crystal thereby increasing the skin depth. In addition, $\eta$ for the layered material decreases close to $T_C$ and becomes unity in the PM phase, which is not true for the small intergrowth component for which $T_C^{IG} \sim 280$ K. Signals from the intergrowth component could be detected up to 200 K with representative spectra shown for an applied field of 1 T in Figs. 5(a) and 5(b). Spectra with significantly larger amplitudes were obtained at 200 K in zero applied field. As mentioned above the magnetization of the intergrowth phase saturates in very low fields resulting in a reduced enhancement factor for this component in applied fields larger than $\sim$0.01 T. Application of a magnetizing field was used to discriminate against signals both from domain walls and intergrowth material. It is worth noting that the spectra above $T_C$, attributed to the 3D intergrowth phase, have a center frequency and linewidth similar to those of 3D polycrystalline LSMO at comparable temperatures, as given in Ref. 32. The center frequency for the intergrowth phase signals occurs at frequencies separated by $\sim$10% for the two field orientations used.

Comparison of these spectral areas with those for spectra at $T<100$ K and allowing for skin depth changes across $T_C$ leads to an estimate of intergrowth concentration less than 0.5% consistent with the estimate given above based on magnetization measurements. Relaxation rate measurements, which are presented below, were made at a number of well-separated frequencies at each temperature to check whether rates were uniform across the spectrum. Similar relaxation

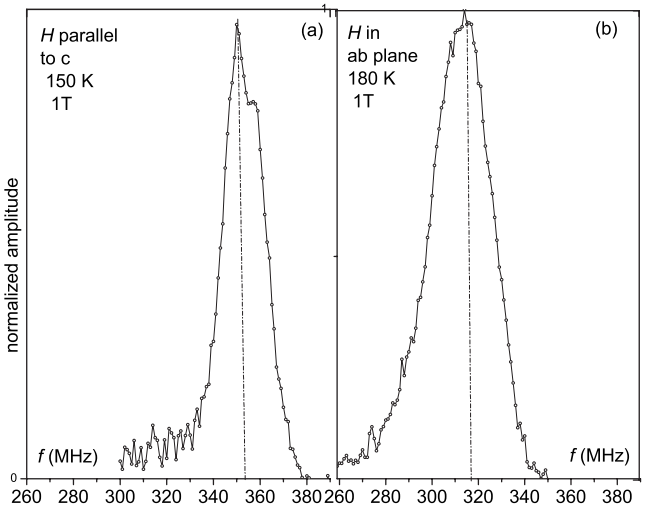


FIG. 5. High-temperature $^{55}$Mn NMR spectra for single crystal $La_{1.2}Sr_{1.8}Mn_2O_7$ with (a) $H$ parallel to the $c$ axis and (b) $H$ in the $ab$ plane. These spectra obtained for $T>T_C$ are much weaker than those obtained at lower temperatures and are attributed to the intergrowth phase with concentration $<0.5\%$ as discussed in the text.

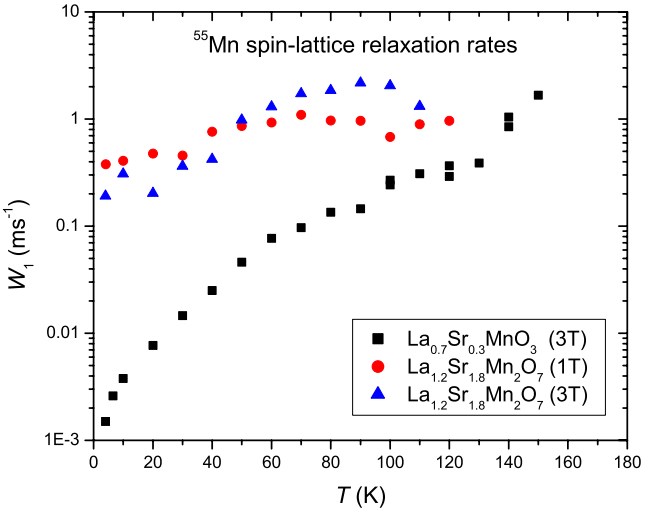


FIG. 6. (Color online) $^{55}$Mn relaxation rates $W_1$ for the bilayered crystal $La_{1.2}Sr_{1.8}Mn_2O_7$ ($\mu_0H=1$ T and 3 T in the $ab$ plane) and for 3D manganite $La_{0.7}Sr_{0.3}MnO_3$ (polycrystalline sample, $\mu_0H=3$ T; Ref. 32) as a function of $T$. For the bilayered system $W_1$ exhibits a much weaker dependence on $T$ than is found in the 3D manganites where a spin-wave mechanism (Ref. 32) is dominant at low $T$.

rates and trends in rates with temperature were found at all frequencies used. This finding provides further evidence that spectra and relaxation rates obtained at temperatures below $T_C$ have negligible contributions from the intergrowth.

## IV. RELAXATION RATES

Because of the large spectral width the relaxation rate measurements involved *hole burning* at particular frequencies in the spectrum demonstrating that the broadening is inhomogeneous. Checks made using a frequency-hopping saturation comb of pulses determined that spectral diffusion is unimportant. The longitudinal nuclear magnetization recovery curves were found to be nonsingle exponential and could be fit either with two exponentials or using the stretched exponential form $M=M_0[1-\exp(-W_1t)^{\beta}]$. From the stretched exponential fits we find that the exponent $\beta$ decreases steadily from 0.5 to 0.3 as $T$ increases from 4 to 100 K for the field in the $ab$ plane. For the field along the $c$ axis $\beta$ remains roughly constant at 0.5 as the temperature is raised. The stretched exponential form implies a distribution of relaxation rates and a decrease in $\beta$ implies a broadening of the distribution. Transverse (spin-spin) relaxation rates $W_2$ were measured using conventional spin-echo techniques and the decay with time was found to be single exponential within experimental uncertainty.

The temperature dependence of the spin-lattice relaxation rate $W_1$ in a field of 1 T (applied in the $ab$ plane for the $La_{2-2x}Sr_{1+2x}Mn_2O_7$ crystal) is much weaker in the bilayered material than in a representative FM 3D LSMO ($x=0.3$) polycrystalline sample[32] as shown in Fig. 6. For $T>100$ K, the $W_1$ values are similar for the two materials, but at lower temperatures $W_1$ for the 3D material decreases more rapidly than in the bilayer crystal. Spin waves play an important role in spin-lattice relaxation in the 3D system with conduction-electron scattering of secondary importance in the temperature range considered.[32]

Figure 7 shows spin lattice $W_1$ and spin-spin $W_2$ relaxation rates as a function of $T$ measured at two different fre-

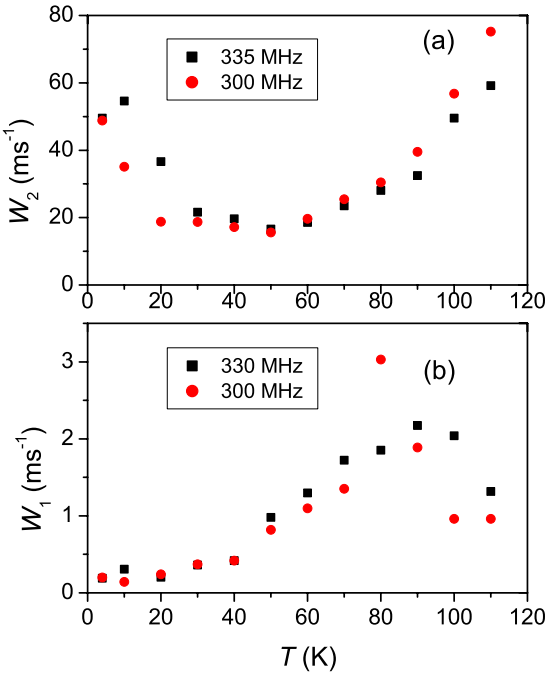


FIG. 7. (Color online) $^{55}$Mn relaxation rates $W_1$ and $W_2$ in $La_{1.2}Sr_{1.8}Mn_2O_7$ as a function of $T$ in the range from 4 to 110 K for $\mu_0H=3$ T in the $ab$ plane. Both quantities exhibit much weaker dependences on $T$ than is found in the 3D manganites (e.g., Ref. 32). $W_2$ exhibits a minimum at 50 K while $W_1$ tends to a roughly constant value below 20 K suggesting that two competing relaxation mechanisms play a role at these temperatures.

quencies in a field of 3 T in the *ab* plane. Similar results (not shown) were obtained for $B$ along $c$ and there is little orientation or frequency dependence of the relaxation rates. $W_1$ has a weak but approximately linear $T$ dependence over part of the range but with marked departures from this behavior below 20 K and above 90 K. $W_2$ exhibits a pronounced minimum around 50 K and is proportional to $T$ between 60 and 110 K. The upturn in $W_2$ below 50 K suggests that longitudinal fluctuations in the hyperfine field become increasingly important in this range. It is interesting to note that the dc electrical resistivity shows a minimum at 50 K.[1] The relationship between the behavior of the NMR transverse relaxation rate and the resistivity in this system requires further investigation. In lower applied fields, including 0 T, the $T$ dependence of the relaxation rates is again rather weak with $W_1$ and $W_2$ showing fairly similar behavior but with $W_2$ more than an order of magnitude larger than $W_1$. The similar trends in $W_2$ and $W_1$ with temperature for $50<T<90$ K point to a common mechanism for the two relaxation processes over this temperature range, with anisotropy in the hyperfine interaction responsible for the enhancement in $W_2$ compared to $W_1$.[32] At temperatures below 40 K anomalous behavior in both $W_2$ and $W_1$ is observed, which suggests a change in the relaxation mechanism in this range.

## V. DISCUSSION

In considering the spectra shown in Figs. 2 and 3 we note that the $^{55}$Mn NMR frequency is due to the isotropic part of the hyperfine interaction is $f=2\pi A\langle S\rangle/\hbar$, where $A$ is the hyperfine coupling and $\langle S\rangle$ the average spin of a Mn ion. By analogy with the 3D manganites the anisotropy is expected to be comparatively small due to double exchange between the $Mn^{3+}(3d^4,S=2)$ and $Mn^{4+}(3d^3,S=3/2)$ ions, which gives rise to a mixed-valence state. The broad spectra shown in Figs. 2 and 3 may be due to residual orbital ordering[27] that produces local variations in the hyperfine field. The fitted Gaussian curves shown in Fig. 3, which are distributed over a range of frequencies, point to variations in $\langle S\rangle$ and/or $A$ at Mn sites.

As can be seen in Fig. 2 the 3D LSMO NMR spectrum is much narrower than that for the bilayer system. This suggests that the electronic structures in these double-exchange FM systems that result in the observed $^{55}$Mn hyperfine fields in the spectra are similar in the 2D and 3D samples but with a much broader distribution in the 2D case. For both magnetic field orientations in the bilayer crystal, changes in the spectral peak frequency with $T$ in the range from 4 to 100 K are comparatively small showing that the hyperfine field distribution is relatively insensitive to temperature changes in this interval. This implies that the average spin $\langle S\rangle$ remains roughly constant over a wide range of $T$ below $T_C$.

The large inhomogeneous linewidths observed below $T_C$ in the present experiments are similar to those observed at helium temperatures in previous $^{55}$Mn NMR experiments on $La_{1.2}Sr_{1.8}Mn_2O_7$.[26,27] The spectral shapes observed in the present work are closer to those found in polycrystalline samples[27] than those seen in the earlier experiments on single crystals where it has been suggested that surface impurity phases may be present.[26] Previous $^{139}$La NMR spectra for crushed single-crystal samples in ZF and in swept applied field (10–15 T), show that the ZF spectra disappear close to $T_c$ but for finite fields spectral shifts with $T$ could be followed up to 300 K, connecting to the ZF spectral shifts at $T_c$.[27] Those authors concluded that there is field-induced FM well above $T_c$. No mention is made of the 3D intergrowth phase that is commonly found to be present in this material. Below $T_c$ the $^{139}$La spectra show little shift with temperature.[26,27] Since the average frequency of a zero-field spectrum is proportional to the magnetization, the $^{139}$La NMR results suggest a first-order FM to PM transition at $T_c$. However, $\mu$SR spectroscopy on $(La_{1-z}Pr_z)_{1.2}Sr_{1.8}Mn_2O_7$ (including $z=0$) has led to conflicting conclusions concerning changes in the hyperfine field with $T$ close to $T_c$.[28] The measured $^{139}$La ZF ($z=0$) spectral shifts again show very little temperature dependence consistent with our $^{55}$Mn data. In contrast, the $\mu$SR data for the muon hyperfine field show behavior typical of a second-order transition with $T_c\sim 105$ K. It has been suggested that this difference in behavior between NMR and $\mu$SR might be explained by exchange coupling between the 3D intergrowth, viewed as stacking faults that are short in the $c$ direction but extended along (001) planes, and the bilayer surroundings.[28] While it would seem likely that samples with less intergrowth should have smaller discrepancy between NMR and $\mu$SR this is not what is observed; the single-crystal data, including our $^{55}$Mn data on a crystal with very small amounts of intergrowth phase, exhibit even weaker temperature dependence of the hyperfine field in the FM phase than powder samples with greater intergrowth concentration. The discrepancy between the NMR and muon data remains unresolved and requires further investigation.

While we cannot draw quantitative conclusions about the microscopic structure of the system from the broad NMR spectra found below $T_C$ qualitative information can be obtained from these data. Structural features present in the spectra shown in Figs. 2 and 3 are not well resolved but the Gaussian fits in Fig. 3 suggest the presence of nonequivalent Mn sites implying some variation in local electronic structure in the sample. In recent $^{55}$Mn NMR experiments on more highly doped $La_{2-2x}Sr_{1+2x}Mn_2O_7$ ($0.5\leq x\leq 1.0$) it has been found that 4.2 K low-field spectra have structural features corresponding to FM and AFM components that depend sensitively on $x$ in the range of 0.5–0.68.[33] In the present $x=0.4$ sample local statistical fluctuations in the Sr doping level could produce significant local changes in the band structure since the magnetic ordering changes from FM to AFM as $x$ increases from 0.4 to 0.45. This change in ordering corresponds to changes in the relative importance of the two $e_g$ states $d_{3z^2-r^2}$ and $d_{x^2-y^2}$.[5,14,34] In addition, the distribution of hyperfine fields may be linked to orbital order effects involving local JT distortions of oxygen octahedra that are static on the NMR time scale.[9–15] In the $La_{2-2x}Sr_{1+2x}Mn_2O_7$ system for $x<0.45$, changes in the Mn $d_{3z^2-r^2}$ orbital occupancy that occur with decreasing $x$ are linked to elongation of the $MnO_6$ octahedra along the apical direction.[2,3,17] Static or long correlation time distortions of this type are not present in the FM phase of 3D manganites.

The relaxation rate results shown in Figs. 6–8 provide additional information on the electronic structure of this ma-

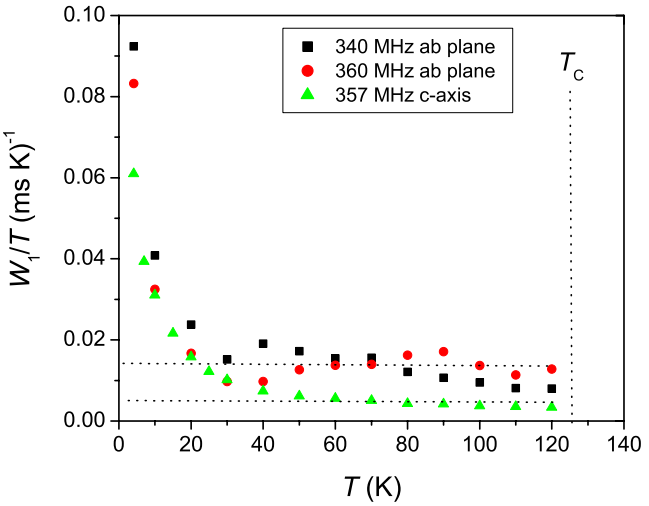


FIG. 8. (Color online) $^{55}$Mn Korringa plot of $W_1/T$ versus $T$ for the $La_{1.2}Sr_{1.8}Mn_2O_7$ crystal with $\mu_0 H=1$ T in the *ab* plane (black squares 340 MHz; red circles 360 MHz) and along the *c* axis (green triangles 357 MHz). The dashed curve shows the region over which the Korringa ratio is approximately constant, as expected for a Fermi liquid, with a clear departure from this behavior found below 20 K.

terial. At temperatures below 40 K anomalous behavior in both $W_2$ and $W_1$ is observed, which suggests a change in the relaxation mechanism in this range. Above 90 K, where the electrical resistivity increases significantly, it is likely that local variations in electronic structure, that grow in importance as $T_c$ is approached, produce departure from Korringa behavior. Large magnetoresistance effects are found in this temperature range and the anomalous spin-lattice relaxation rate behavior suggests that this effect is due to the emergence of polarons that play a key role in magnetoresistance. The magnetic field dependence of $W_1$ that is evident above 90 K in Fig. 6 provides support for this interpretation.

Figure 8 gives a plot of the $^{55}$Mn ratio $W_1/T$ versus $T$ for an applied field of 1 T both in the *ab* plane and along the *c* axis. The 3 T *ab* plane data give a similar plot with somewhat more pronounced sigmoid shape in the temperature interval 30 to 90 K. The behavior is clearly unconventional for a metal. There is an interval where Korringa relaxation applies, at least approximately with $W_1 \propto T$ but significant departures from this relationship occur at both low and high temperatures. The general expression for the nuclear relaxation rate due to a fluctuating hyperfine interaction is[35]

$$W_1 = \frac{2\gamma_I^2 T}{N}\sum_q |A_q|^2 \frac{\chi''_\perp(q,\omega_0)}{\omega_0}, \tag{1}$$

where $\gamma_I$ is the nuclear gyromagnetic ratio, $A_q$ is the hyperfine coupling corresponding to wave vector $q$, $N$ is the number of magnetic ions per unit volume, $\chi''_\perp(q,\omega_0)$ is the transverse component of the imaginary part of the magnetic susceptibility, and $\omega_0$ is the resonance frequency.[35] In view of the lack of knowledge of $\chi''_\perp(q,\omega_0)$ in this system we adapt available expressions for 3D FM. In order to allow for competing relaxation mechanisms we write the relaxation rate as the sum of several contributions $\alpha$ as follows $W_1 = \Sigma_\alpha W_1^\alpha$. The various contributions that need consideration are discussed below.

In a FM metal the most important relaxation mechanisms are conduction-electron scattering and spin-wave scattering. The relaxation rate due to spin waves in a quasi-2D FM is obtained by generalizing the perturbation theory approach used for 3D systems[32,36] through replacement of the 3D density of states (DOS) with the 2D density of states for spin-wave excitations. Neutron scattering has shown that the spin-wave dispersion is close to 2D with in-plane stiffness $D \sim 151$ meV Å. The nuclear relaxation rate for a Raman two-magnon process, involving the annihilation of excitation $q$ and the creation of $q'$ with an energy difference $AS$ due to the nuclear-spin flip, and mediated by the component $A_\perp$ of the anisotropic contact hyperfine interaction $A$, is[36]

$$W_1^{sw} = 2(2\pi/\hbar)(A_\perp/2N)^2 \sum_{q,q'} n_{q'}(1+n_q)\delta(E_q - E_{q'} - AS). \tag{2}$$

$N$ is the number of spins and the populations $n_k, n_{k'}$ are given by the Bose-Einstein distribution. Replacing the sum by integrals over $q$ we obtain

$$W_1^{sw} = 2(2\pi/\hbar)(A_\perp/2N)^2 (Na^2/4\pi^2)^2 4\pi^2 \times \int\int qdqq'dq' \left[\frac{e^{E_q/k_BT}}{(e^{E_q/k_BT}-1)^2}\right]\delta(E_q - E_{q'}),$$

where $a$ is the lattice constant in the 2D FM. Based on the neutron-scattering results for $x=0.4$,[17,18] we choose the following form for the dispersion relation $E_q = g\mu_B H + 2JSq^2a^2$. Defining $\hbar\omega_e = 2JS$ and integrating by parts gives

$$W_1^{sw} = (1/16\pi)(A_\perp^2 k_B^2/\hbar^3\omega_e^2 g\mu_B H)T^2. \tag{3}$$

In zero or low applied fields $H$ is the anisotropy field. Estimating $\hbar\omega_e \approx 10$ meV using the in-plane spin-wave stiffness constant from neutron scattering leads to $W_1^{sw} \sim (1.4\times10^4 \sin^2\alpha)T^2$ s$^{-1}$. Here $\alpha$ is the angle between the $S$ spin and the $I$ spin-quantization axes due to hyperfine anisotropy.[32] The predicted quadratic $T$ dependence given by Eq. (3) is not observed experimentally showing that, in contrast to the 3D FM manganite case,[32] the two-magnon mechanism is not the relaxation rate determining the process in $La_{2-2x}Sr_{1+2x}Mn_2O_7$.

As noted in the introduction, considerable evidences suggest that the FM phase of $La_{2-2x}Sr_{1+2x}Mn_2O_7$ is not a conventional Fermi liquid.[19–22] Nevertheless, as a starting point for comparison purposes we consider relaxation in this quasi-2D system using expressions that apply to spin-polarized 3D Fermi liquids. For FM metals the conduction-electron contribution to the spin-lattice relaxation rate may be written as

$$W_1^{ce} = (16\pi/5)\gamma_I^2\hbar k_B T\langle A^{orb}\rangle_F^2 \rho_\uparrow^2(E_F) F^{orb}(\Gamma). \tag{4}$$

$\langle A^{\mathrm{orb}}\rangle_F$ is the $d$-electron orbital hyperfine interaction averaged over the Fermi surface, and $\rho_{\uparrow}^2(E_F)$ is the square of the majority spin band density of states at the Fermi level.[32] The factor $F^{\mathrm{orb}}(\Gamma)$ depends on the admixture of $t_{2g}(\Gamma_5)$ and $e_g(\Gamma_2)$ $d$-electron states at the Fermi surface and has a maximum value of unity.[32] Eq. (4) predicts that $W_1/T$ should be temperature independent and, as shown in Fig. 8, this prediction is found to hold approximately over the range of 30–90 K with large deviations occurring at low $T$.

Considerable evidences have been obtained showing that the Fermi surface in $La_{2-2x}Sr_{1+2x}Mn_2O_7$ is similar in some respects to that of the high-$T_C$ cuprates.[20,21] Nesting of parallel parts of the Fermi surface leads to a loss in spectral weight, or pseudogap, at the Fermi level. ARPES experiments suggest that LSMO is a polaronic metal in which polaron condensation induced by DE occurs as the temperature decreases through $T_C$.[20,21] A sharp quasiparticle peak found along the (0,0) to $(\pi,\pi)$ nodal direction at low temperatures collapses above 86 K.[20,21] NMR relaxation rate results for the cuprates and other correlated electron systems exhibit significant departures from Korringa behavior in certain regions of their phase diagrams.[35] The present results show that $La_{2-2x}Sr_{1+2x}Mn_2O_7$ ($x=0.4$) is a further example of a correlated system in which non-Korringa behavior is found in NMR relaxation.

For metallic 3D LSMO ($x=0.3$), assuming $F^{\mathrm{orb}}(\Gamma)\sim 1$, Eq. (4) predicts as an upper limit value for the ratio $W_1^{\mathrm{ce}}(3D)/T\sim 1.2\ \mathrm{s}^{-1}\ \mathrm{K}^{-1}$. The experimental value of this ratio for 3D LSMO is roughly an order of magnitude smaller than this and the lack of agreement may, at least in part, be attributed to an uncertainty in $F^{\mathrm{orb}}(\Gamma)$.[32] The corresponding measured ratio in $La_{2-2x}Sr_{1+2x}Mn_2O_7$ for $T>40$ K is, from Fig. 8, $W_1^{\mathrm{ce}}(2D)/T=0.015\pm 0.005\ \mathrm{s}^{-1}\ \mathrm{K}^{-1}$. Examination of Fig. 6 shows that a detailed comparison of the relaxation mechanisms for the 2D and 3D manganites based on Eqs. (3) and (4) is not simple to make. For the 3D LSMO, spin waves mediated by the anisotropic hyperfine coupling, provide the dominant relaxation mechanism for $T<100$ K, while they do not appear to play a major role in the $x=0.4$ bilayered quasi-2D material, although it is likely that some contribution to relaxation comes from this source. The unexpectedly low value found for $W_1^{\mathrm{ce}}(2D)/T$ above 40 K suggests that changes in the electronic structure with temperature result in variations with temperature of one or more of the parameters $\langle A^{\mathrm{orb}}\rangle_F$, $\rho_{\uparrow}^2(E_F)$, and $F^{\mathrm{orb}}(\Gamma)$ involved in Eq. (4). Lack of knowledge of the behavior of these parameters with $T$ prevents quantitative comparative analysis of the 2D and 3D relaxation rates.

Below 40 K the Korringa plot in Fig. 8 shows anomalous behavior that may be attributed to either some new competing relaxation mechanism becoming dominant at these temperatures in this poor metal, or to a significant increase in the DOS at the Fermi level and/or in the factor $F^{\mathrm{orb}}(\Gamma)$ with decreasing $T$. An increase in the DOS would imply a decrease in the conduction bandwidth, while changes in $F^{\mathrm{orb}}(\Gamma)$ correspond to an increase in the $t_{2g}$ character of the wave function at the Fermi surface. In terms of susceptibility the almost constant value of $W_1$ implies that in Eq. (1) $\chi_{\perp}''(q,\omega_0)\propto 1/T$ below 40 K. The relaxation rates are sufficiently short ($\sim$2.5 ms) that it is unlikely that a powerful competing mechanism will emerge at such comparatively low temperatures. Two-magnon processes, as considered above, would not lead to the observed behavior nor would the two-phonon processes. The activation energy for polaron hopping above $T_C$ is $\sim$68 meV (Ref. 15) and it is not plausible that a polaron hopping mechanism will contribute to relaxation at low temperatures. It is, however, possible that small lattice distortions linked to changes in orbital ordering could lead to changes in the electronic structure. A two-band model involving both localized JT polaronic levels and delocalized band states has been proposed to account for the CMR properties of manganites.[37] This approach stresses the importance of JT electron-lattice couplings, which could be important in determining the relaxation rate behavior. It is of interest to consider the resistivity $\rho$, which shows a weak dependence on $T$ and $H$ below $T_C$ and has a slight upturn below 30 K, where the nuclear relaxation rate anomaly appears. In order to account for the low-$T$ behavior of $\rho$ it has been suggested that weak localization of carriers and also electron-electron interaction effects may be important in this quasi-2D system.[23] It is, however, unclear whether these effects, or small JT lattice displacements linked to orbital ordering changes, can account for the anomalous relaxation behavior that is observed at low temperatures in the bilayer system. Finally, as mentioned above, the anomalous relaxation rate behavior found between 90 K and $T_C$ provides evidence for the emergence of polarons consistent with the large magnetoresistance effects found in this temperature range.

## VI. CONCLUSION

$^{55}$Mn NMR spectra obtained in the FM phase of the bilayered manganite $La_{1.2}Sr_{1.8}Mn_2O_7$ show a broad distribution of hyperfine couplings consistent with local lattice disorder in this system. The hyperfine field distribution may be linked to static JT distortions that persist below $T_C$ as local-orbital ordering. In addition, considerations based on the phase diagram for $La_{2-2x}Sr_{1+2x}Mn_2O_7$ in the region $x\sim 0.4$ suggest that statistical fluctuations in the dopant concentration can lead to local variations in the electronic structure due to changes in relative importance of the $d_{x^2-y^2}$ and $d_{3z^2-r^2}$ orbitals with $x$. Nuclear spin-lattice relaxation rate results suggest that, in contrast to FM 3D LSMO ($x=0.3$), spin waves play no detectable role in relaxation. In the FM metallic phase electron scattering provides the dominant relaxation mechanism at temperatures well below $T_C$, where weak Korringa-type behavior is found in this poorly metallic system over the range of 40–90 K. The observation of a major departure from Korringa behavior below 40 K is likely due to changes either in the DOS at the Fermi level or in the wave function at the Fermi surface caused by changes in electron-lattice coupling linked to local changes in orbital ordering. Above 90 K we suggest that the growing importance of polarons, which play a role in the magnetoresistance properties, is responsible for the anomalous field-dependent decrease in the relaxation rate.

**ACKNOWLEDGMENTS**

Financial support for the work at the NHMFL was provided through grants from the NSF (Grant No. DMR-0084) and by the state of Florida. The work at Argonne National Laboratory was supported by the U.S. DOE, Office of Science, Basic Energy Sciences, under Contract No. DE-AC02-06CH11357. Helpful discussions with Pedro Schlottmann at Florida State University and Chris Leighton at the University of Minnesota are gratefully acknowledged.

[1] Y. Moritomo, A. Asamitsu, H. Kuwahara, and Y. Tokura, Nature (London) **380**, 141 (1996).
[2] J. F. Mitchell, D. N. Argyriou, J. D. Jorgensen, D. G. Hinks, C. D. Potter, and S. D. Bader, Phys. Rev. B **55**, 63 (1997).
[3] D. N. Argyriou, J. F. Mitchell, P. G. Radaelli, H. N. Bordallo, D. E. Cox, M. Medarde, and J. D. Jorgensen, Phys. Rev. B **59**, 8695 (1999).
[4] T. Kimura, Y. Tomioka, A. Asamitsu, and Y. Tokura, Phys. Rev. Lett. **81**, 5920 (1998).
[5] Q. Zhang, W. Zhang, and Z. Jiang, Phys. Rev. B **72**, 142401 (2005).
[6] M. W. Kim, H. J. Lee, B. J. Yang, K. H. Kim, Y. Moritomo, J. Yu, and T. W. Noh, Phys. Rev. Lett. **98**, 187201 (2007).
[7] C. D. Potter, M. Swiatek, S. D. Bader, D. N. Argyriou, J. F. Mitchell, D. J. Miller, D. G. Hinks, and J. D. Jorgensen, Phys. Rev. B **57**, 72 (1998).
[8] D. N. Argyriou, J. F. Mitchell, C. D. Potter, S. D. Bader, R. Kleb, and J. D. Jorgensen, Phys. Rev. B **55**, R11965 (1997).
[9] L. Vasiliu-Doloc, S. Rosenkranz, R. Osborn, S. K. Sinha, J. W. Lynn, J. Mesot, O. H. Seeck, G. Preosti, A. J. Fedro, and J. F. Mitchell, Phys. Rev. Lett. **83**, 4393 (1999).
[10] G. M. Zhao, V. Smolyaninova, W. Prellier, and H. Keller, Phys. Rev. Lett. **84**, 6086 (2000).
[11] A. S. Alexandrov, A. M. Bratkovsky, and V. V. Kabanov, Phys. Rev. Lett. **96**, 117003 (2006).
[12] B. J. Campbell, R. Osborn, D. N. Argyriou, L. Vasiliu-Doloc, J. F. Mitchell, S. K. Sinha, U. Ruett, C. D. Ling, Z. Islam, and J. W. Lynn, Phys. Rev. B **65**, 014427 (2001).
[13] B. J. Campbell, S. K. Sinha, R. Osborn, S. Rosenkranz, J. F. Mitchell, D. N. Argyriou, L. Vasiliu-Doloc, O. H. Seeck, and J. W. Lynn, Phys. Rev. B **67**, 020409(R) (2003).
[14] T. Ohsawa and J. I. Inoue, Phys. Rev. B **65**, 134442 (2002).
[15] S. Miyaki, S. Uzuhara, K. Terada, K. Makoshi, and H. Koizumi, Phys. Rev. B **71**, 085117 (2005).
[16] H. Fujioka, M. Kubota, K. Hirota, Y. Yoshizawa, Y. Moritomo, and Y. Endoh, J. Phys. Chem. Solids **60**, 1165 (1999).
[17] T. G. Perring, D. T. Adroja, G. Chaboussant, G. Aeppli, T. Kimura, and Y. Tokura, Phys. Rev. Lett. **87**, 217201 (2001).
[18] K. Hirota, S. Ishihara, H. Fujioka, M. Kubota, H. Yoshizawa, Y. Moritomo, Y. Endoh, and S. Maekawa, Phys. Rev. B **65**, 064414 (2002).
[19] P. E. Mijnarends, S. Kaprzyk, B. Barbiellini, Y. Li, J. F. Mitchell, P. A. Montano, and A. Bansil, Phys. Rev. B **75**, 014428 (2007).
[20] N. Manella, W. L. Yang, X. J. Zhou, H. Zheng, J. F. Mitchell, J. Zaanen, T. P. Devereaux, N. Nagaosa, Z. Hussain, and Z.-X. Shen, Nature (London) **438**, 474 (2005).
[21] N. Mannella, W. L. Yang, K. Tanaka, X. J. Zhou, H. Zheng, J. F. Mitchell, J. Zaanen, T. P. Devereaux, N. Nagaosa, Z. Hussain, and Z.-X. Shen, Phys. Rev. B **76**, 233102 (2007).
[22] D. S. Dessau, T. Saitoh, C.-H. Park, Z.-X. Shen, P. Villella, N. Hamada, Y. Moritomo, and Y. Tokura, Phys. Rev. Lett. **81**, 192 (1998).
[23] A. A. Abrikosov, Phys. Rev. B **61**, 7770 (2000).
[24] R. H. Heffner, D. E. MacLaughlin, G. J. Nieuwenhuys, T. Kimura, G. M. Luke, Y. Tokura, and Y. J. Uemura, Phys. Rev. Lett. **81**, 1706 (1998).
[25] A. I. Coldea, S. J. Blundell, C. A. Steer, J. F. Mitchell, and F. L. Pratt, Phys. Rev. Lett. **89**, 277601 (2002).
[26] K. Shimizu, M. Velázquez, J. P. Renard, and A. Revcolevschi, J. Phys. Soc. Jpn. **72**, 793 (2003).
[27] G. Allodi, M. Bimbi, R. De Renzi, C. Baumann, M. Apostu, R. Suryanarayanan, and A. Revcolevschi, Phys. Rev. B **78**, 064420 (2008).
[28] Y. Shiotani, J. L. Sarrao, and G. Q. Zheng, Phys. Rev. Lett. **96**, 057203 (2006).
[29] U. Welp, A. Berger, V. K. Vlasko-Vlasov, Q. A. Li, K. E. Gray, and J. F. Mitchell, Phys. Rev. B **62**, 8615 (2000).
[30] T. Asaka, T. Kimura, T. Nagai, X. Z. Yu, K. Kimoto, Y. Tokura, and Y. Matsui, Phys. Rev. Lett. **95**, 227204 (2005).
[31] J. Huang, C. Hyun, T.-M. Chuang, J. Kim, J. B. Goodenough, J.-S. Zhou, J. F. Mitchell, and A. de Lozanne, Phys. Rev. B **77**, 024405 (2008).
[32] M. J. R. Hoch, P. L. Kuhns, W. G. Moulton, A. P. Reyes, M. A. Torija, J. F. Mitchell, and C. Leighton, Phys. Rev. B **75**, 104421 (2007).
[33] D. Rybicki, C. Kapusta, W. Tokarz, H. Štěpánková, V. Procházka, J. Haase, Z. Jirák, D. T. Adroja, and J. F. Mitchell, Phys. Rev. B **78**, 184428 (2008).
[34] R. Saniz, M. R. Norman, and A. J. Freeman, Phys. Rev. Lett. **101**, 236402 (2008).
[35] T. Moriya and K. Ueda, Rep. Prog. Phys. **66**, 1299 (2003).
[36] D. Beeman and P. Pincus, Phys. Rev. **166**, 359 (1968).
[37] T. V. Ramakrishnan, H. R. Krishnamurthy, S. R. Hassan, and G. Venketeswara Pai, Phys. Rev. Lett. **92**, 157203 (2004).